Journal of Solid Mechanics Vol. 15, No. 1 (2023) pp. 66-77
DOI: 10.22034/jsm.2021.1938200.1714

Research Paper

Selection of Optimal Tool Geometry for the Production of Brass Wires Using the FSBE Method

M. Akbari [1,*], P. Asadi [2], H. Rahimi Asiabaraki [1]

[1]*Department of Mechanical Engineering, Technical and Vocational University (TVU),Tehran, Iran*
[2]*Department of Mechanical Engineering, Faculty of Engineering, Imam Khomeini International University, Qazvin, Iran*

Received 28 September 2022; accepted 14 December 2022

ABSTRACT

This research studied different tools with different cone angles to produce brass wires using the friction stir back extrusion (FSBE) method. The cone angle of the tool is one of the most influential parameters in the production of brass wires. First, to determine the appropriate cone angle, the FSBE process is modeled using the Coupled Eulerian-Lagrangian (CEL) method. The simulation results showed that increasing the cone angle increases the heat generated and reduces the force on the tool. Also, to be more precise, the mechanism of heat production during the process was numerically modeled to verify the simulation results. The cross-sectional images of the wires produced showed that only tools with a cone angle of 35 ° could produce flawless wires. The microstructural results showed that the grain size in the center of the wire was 20.24 microns, which is larger than the size in the wire periphery, which was 16.88 microns. This microstructural deviation is mainly affected by the strain and the temperature.

Keywords : FSBE; Recycling; Microstructure; FEM; Cone angle.

1 INTRODUCTION

BRASS is generally composed of 5 to 45% zinc, which increases the hardness of this alloy, and the rest is composed of copper, which improves the corrosion resistance of this alloy [1,2]. Therefore, the mechanical properties of these alloys are entirely dependent on the amount of zinc and copper in them. Furthermore, brasses have high thermal and electrical conductivities, high malleability, a good combination of strength and ductility, high corrosion resistance, good castability and formability, and excellent machinability [3,4]. These alloys' amazing and unique properties have led to widespread use in various fields, such as counters and taps, bearings, plumbing fittings and fixtures, and low-pressure valves. Due to limited resources, environmental protection, and energy-saving, metal recycling has attracted the attention of many countries. Alloys such as copper, brass, and aluminum, which are widely used in various industries, are one of the largest sources of metal loss due to the machining process and the production of metal chips. Traditionally, these chips are melted and reused. In this way, some companies are needed to collect the chips and transfer them to the casting shops, and rolling, extrusion, and other processes are required to

*Corresponding author.
E-mail address: Mo-akbari@tvu.ac.ir (M. Akbari)

produce the final/usable metal product. The advent of new recycling methods such as Friction Stir Back Extrusion (FSBE) has led to the recycling of these alloys directly to the product[5,6]. Many researchers have already demonstrated the capabilities of friction-based processes such as the friction stir welding (FSW) process in metal joining [7-9]. Recently, a friction-based process has been developed to recycle metal chips called FSBE. The FSBE as a solid-state recycling technique produces frictional heat to soften the recycled chips, and then, by applying adequate pressure as a forging force, the chips are merged and pushed into a channel to produce an integrated product like a wire or tube [10]. So far, research has been done to evaluate the performance of this process. Li et al. [11] fabricated Mg-RE alloys with high strength and ductility using FSE. Baffari et al. [12] examined various process parameters, including tool rotation, rate extrusion ratio, and force, during the FSB process. They concluded that extrusion rate directly influences the product's surface quality. Asadi et al. [13] studied the behavior of the material flow during the process. They stated that the material flow pattern is a conical helix, and changing process parameters has no effect on the material flow pattern. In another study, Akbari et al. [14] studied the process parameters, including linear velocity and tool rotational speed, and then obtained the optimal values of these parameters using the Taguchi method.

Although studies on the production of wire from chips by the FSBE method have been done so far, tool design in this process, which plays a vital role in the quality of products produced, has not been studied. In this research, the tool cone angle, which is one of the most critical parameters of the tool, has been studied. In order to explore more precisely the effect of the tool cone angle on the process, the FSBE process was simulated using the CEL method. The model is validated based on the acquired experimental temperature data. After selecting the optimal tool, the mechanical and microstructural properties of the produced wires were studied.

2 EXPERIMENTAL PROCEDURE

The experimental setup is made up of three essential components: a rotational tool, a matrix that serves as a chip storage area, and some raw material in the form of chips or bulk. The matrix is firmly attached to the milling machine table. The tool surface in touch with the material is sloped to guide the material into the central hole better. The chips are put inside the matrix during this procedure. After then, the rotating tool enters the matrix with a set traversal speed. The rotation and translation along the feed direction generate a large quantity of friction-induced heat, which softens and thoroughly consolidates the chips. The softened chips are fed into the instrument and emerge as wires.

The tool head contains a conical concave toward the central hole for a more effortless flow of softened material from the primary material toward the sizing channel for the wire. A brass shaft with a diameter and height of 30 and 40 *mm*, was used as the primary bulk material.

In this research, a CuZn39Pb2Sn brass shaft with the chemical composition listed in Table 1 was used to perform the FSBE process. The metal matrix was made of H13 steel and then subjected to heat treatment. The hardness of the metal matrix was 52 *HV* after heat treatment. The FSBE tools with an inner diameter of 7 *mm* and an outer diameter of 30 *mm* were made of Chrome-Nickel steel and subjected to heat treatment. The tool heads contain three different cone angles of 15 º, 25 º, and 35º toward the central hole for a more effortless flow of softened material from primary material toward the sizing channel for the wire (Fig. 1). In order to produce wires, a rotational speed of 800 *rpm* and a linear speed of 40 *mm/min* were used. The process setup is shown in Fig. 2(a).

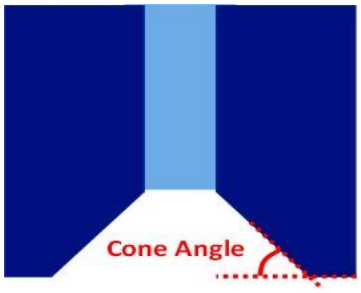

Fig.1
The cone angle in the FSBE tool.

In order to validate the numerical model, a four-channel thermometer was used to acquire the temperature history during the process, and the thermocouples were embedded in the matrix body.

In order to study the microstructure of the produced wires, the cross-section of the wires was polished and etched, and their microstructure was analyzed using a light microscope. The prepared metallographic samples are etched with a solution of 5 *g* Fe_3Cl, 30 *mL* HCl and 100 *mL* ethanol for 20 seconds and then washed with distilled water and dried.

Table 1
Chemical compositions of CuZn39Pb2Sn brass used in this study.

Element	Cu	Zn	Pb	Sn	Fe	Ni	Al	Mn	Si	S	P
% wt.	58.9	37.39	2.14	0.60	0.51	0.43	0.007	0.004	0.003	0.003	0.003

The hardness of the samples was measured at two points, the center and the periphery of the wire. The hardness test was measured with a load of 100 *g* for 15 seconds. The standard pressure test was performed at ambient temperature with a strain rate of 10-3 s-1 using Cometech universal tensile/pressure test equipment. The length of pressure test specimens was 12 *mm*. Fig. 2(b) shows the pressure test setup.

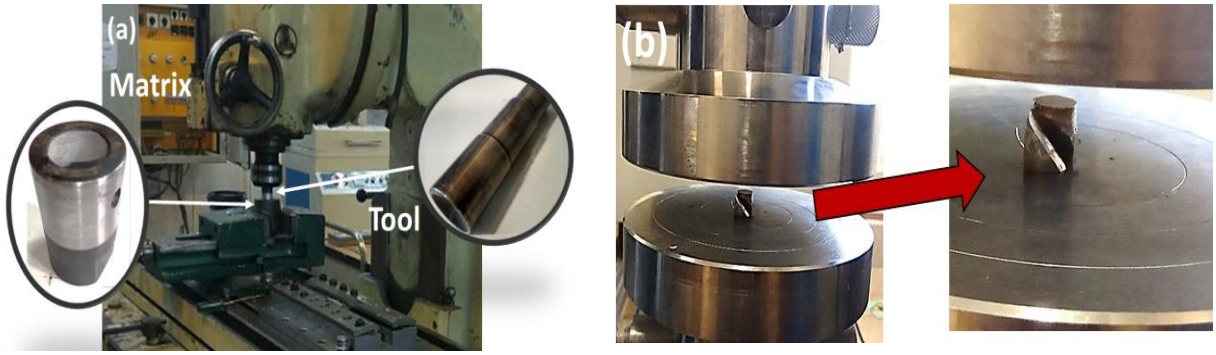

Fig.2
(a) The FSBE process setup; used in this investigation, (b) The pressure test.

3 MODEL DESCRIPTION

The ABAQUS software was used to simulate the temperature and force history during the FSBE. The Coupled Eulerian-Lagrangian (CEL) method was employed in this investigation to simulate the FSBE process. In this method, the finite elements are fixed, and materials can pass through these elements. For this reason, there are no problems such as excessive distortion of the elements, which occurs in other methods such as ALE during severe plastic deformation. The FSBE tool is defined as a rigid Lagrangian body, and the material was described as an Eulerian part with EC3D8RT elements. The Eulerian part was modeled as a cylinder consisting of two sub-regions, "void" and "full". A brass alloy was assigned to the "full" region while the "void" area was left empty to allow material to move during the process. The material layout used in the present model to produce the brass wires is shown in Fig. 3.

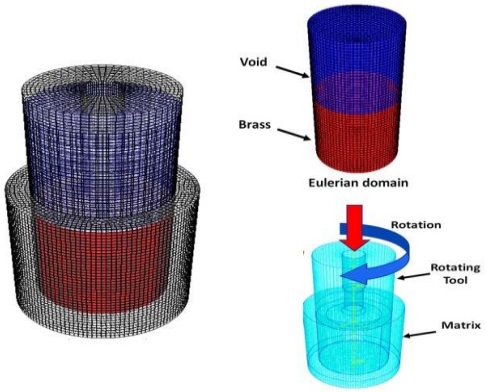

Fig.3
The material layout used in the present model for FSBE to produce the brass wires.

3.1 Governing equations

The workpiece domain is modeled using the CEL approach proposed in this paper, which uses an Eulerian formulation in which energy, mass, and momentum are conserved.

The mass conservation equation represents the rate of outflow mass and mass variations inside the control volume (Eq. (1)).

$$\frac{\partial \rho}{\partial t} + \nabla.(\rho v) = 0 \tag{1}$$

where ρ and v are the density and velocity of the material, respectively, the conservation equation for momentum (Eq. (2)) equals the change of momentum of the domain to the sum of the spatial time derivative of the gravitational force and the Cauchy stress tensor.

$$\rho(\frac{\partial v}{\partial t} + \nabla.(v \otimes v)) = \nabla.\sigma + \rho g \tag{2}$$

where σ and g are the Cauchy stress tensor and the gravity constant, the energy conservation equation incorporates the rate of plastic work done on any element, the heat flux into elements as a result of conduction, and the generation of the volumetric heat from the element.

$$\rho C_p(\frac{\partial T}{\partial t} + v.\nabla T) = \nabla.(K\nabla T) + \nabla.(\sigma v) + \dot{Q} \tag{3}$$

where K, Cp, T, and Q denote thermal conductivity, material-specific heat, Kelvin temperature, and volumetric heat generation rate, respectively. The following is the general conservation form of the Eulerian-based equations (Eqs. (1-3)):

$$\frac{\partial \phi}{\partial t} + \nabla.\Phi = S \tag{4}$$

where S and Φ are the source term and the flux function, respectively. The Operator splitting algorithm splits the governing equation (Eq. (4)) into Eulerian steps containing the flux function term Φ and a Lagrangian step containing the source term S, as shown in Eqs. (5) and (6). These two equations were solved consecutively using the CEL method. The split operator is shown schematically in Fig. 4 for each step of the CEL method.

$$\frac{\partial \varphi}{\partial t} = S \tag{5}$$

$$\frac{\partial \varphi}{\partial t} + \nabla.\Phi = 0 \tag{6}$$

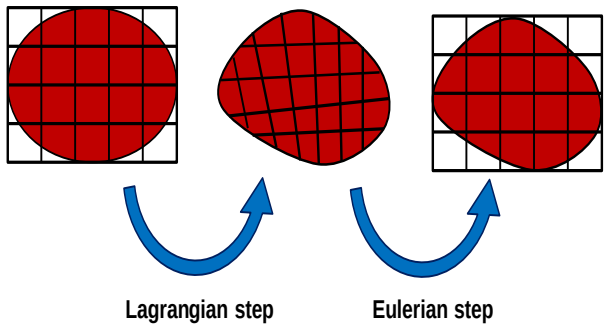

Fig.4
The split operator used in the CEL method.

3.2 Material model

Temperature, strain rate, and strain are all factors that influence the material flow stress in the process. Therefore, Johnson-Cook's model (JC) is utilized to model the flow of material:

$$\sigma = (A + B\,\varepsilon^{n})(1 + C\,\ln\left(\frac{\dot{\varepsilon}}{\dot{\bar{\varepsilon}}}\right))[1 - \left(\frac{(T - T_r)}{(T_m - T_r)}\right)^{m} \tag{7}$$

where A, B, C, n, and m are constants related to the material, T_m is melting temperature (from Table 2); T_r is the ambient temperature, ε represents the plastic strain; $\dot{\bar{\varepsilon}}$ the normalizing strain rate; and $\dot{\varepsilon}$ is the effective plastic strain rate [15, 16]. Eq. (7) first term is the power law, which describes how plastic training affects flow stress. The effects of strain rate and temperature were examined in the second and third terms of the equation. Table 2 illustrates Johnson-Cook's parameters for brass alloys [15].

Table 2
The constants of JC model for the AA 5083 and brass alloys[15].

Material	A [MPa]	B [MPa]	C	n	m	T_{ref} [$°C$]	T_{melt} [$°C$]
Brass	112	505	0.009	0.42	1.68	25	916

3.3 Contact interactions and boundary conditions

Plastic deformation and friction are the principal sources of heat creation during FSBE, with Q_F and Q_P representing friction and plastic heat generation, respectively. Eq. (9) expresses friction heat generation as the tangential stress and slip-rate product at the interface. Furthermore, as indicated in Eq. (10), the degree of material deformation impacts the quantity of heat generated by plastic deformation.

$$\dot{Q}_F = \phi(\tau_S \times \dot{\gamma}) \tag{8}$$

$$\dot{Q}_P = \eta(\sigma \times \dot{\varepsilon}) \tag{9}$$

where σ is flow stress, ϕ is frictional heat factor, ε represents strain-rate, η is inelastic heat fraction, and $\dot{\gamma}$ is slip-rate, respectively. Moreover, heat dissipation because of convection occurred from the workpiece surfaces to the air:

$$-K\,\frac{\partial T}{\partial \delta_S} = \gamma_{con}\,(T - T_a) \tag{10}$$

where T_a and γ_{con} represent the peripheral temperature and the coefficients of heat convection. A convective heat transfer coefficient is used to model the natural convection heat loss at the matrix and paunch outer surfaces. In addition to the FSBE paunch/workpiece contact, the materials in the process have a self-contact. A general contact interaction can be utilized to account for all contact points between the workpiece and the tool. The friction between the tool and the substance is represented using the Coulomb friction model. The hard contact pressure enclosure also simulates typical tool-to-material contact, reducing workpiece node penetration into the tool.

3.4 Meshing

Thermally coupled eight-node linear Eulerian brick elements (EC3D8RT) with reduced integration are used to mesh the Eulerian domain. A fine mesh is an important parameter to consider while creating an accurate FSBE model. Furthermore, a coarse mesh causes Eulerian material to flow through the Lagrangian mesh [10]. A fine mesh with a mesh size of 0.8 *mm* was chosen after testing several mesh sizes (Fig. 5). The matrix and FSBE tool are meshed using thermally coupled 4-node 3D bilinear rigid quadrilateral elements and treated as a Lagrangian rigid body. The mesh size of 2 mm and 1.5 mm were utilized to mesh matrix and tool, respectively [8]. By specifying the tool reference point, all tool movements were assigned to this point to precisely control the tool.

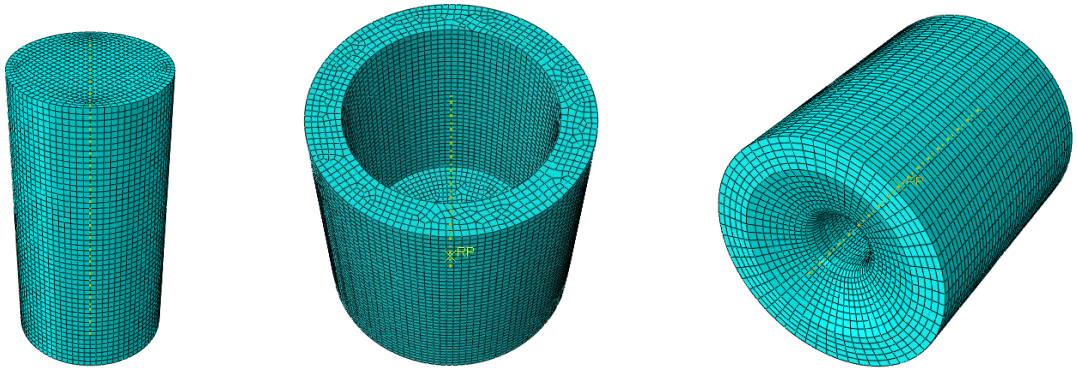

(a) (b) (c)

Fig.5
Mesh in the CEL model: (a) Eulerian mesh for the workpiece, (b) Lagrangian mesh for the matrix, and (c) Lagrangian mesh for the tool.

4 RESULTS

First, the effects of cone angle were investigated using numerical methods, and after selecting the optimal tool, the wires were produced, and their microstructural and mechanical properties were investigated.

4.1 Numerical model validation

In order to validate the numerical model, the temperature obtained experimentally was compared with the numerical results. (Fig. 6). Temperatures are taken on the matrix body at a distance of 3 *mm* from the inside cylindrical surface and 10 *mm* from the top surface. The temperature distribution on the matrix body is shown in Fig. 6(a) when the tool is penetrated almost 10 *mm* on the matrix hole (5 *mm* into the workpiece) at 800 *rpm* and 25 *mm/min*.

As it turns out, there is an excellent agreement between the numerical and experimental results, which indicates the model's capacity in process simulation. Although the highest temperature in the matrix body reaches over 600 °*C*, the temperature in the tool/workpiece interface is substantially higher.

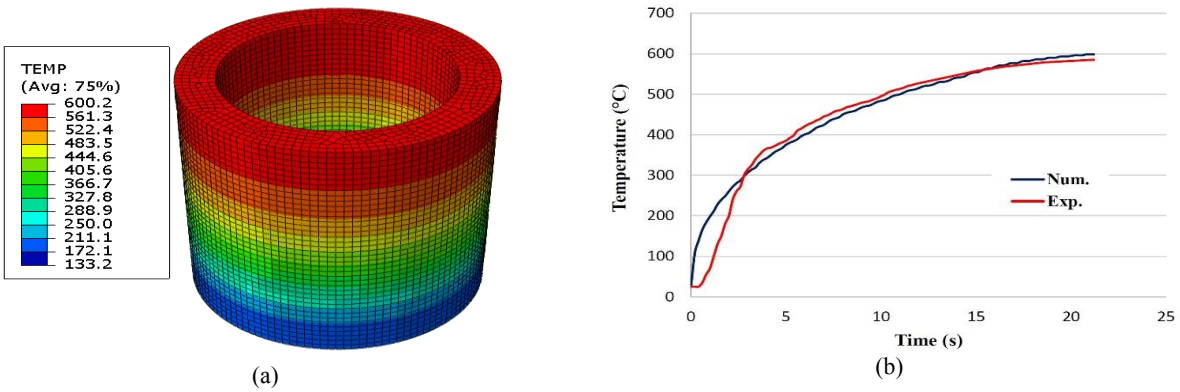

(a) (b)

Fig.6
(a) The temperature distribution in the matrix body over the FSBE process; the tool is penetrated 5 *mm* into the workpiece. (b) The experimental and numerical temperature history curves.

4.2 Select the optimal FSBE tool

Fig. 7 shows the temperature distribution in samples produced with different tools. In the FSBE process, similar to other friction-based processes, the heat required during the process is provided by the friction between the material and the tool. Then by deformation of the material during the process, the plastic deformation heat is added to the

total generated heat. Since this process is a solid-state process, the temperature in the material is about 60 to 90% of the melting temperature [17, 18]. Rising material temperatures cause the materials to soften, and by applying axial force, the softened materials deform and enter the tube. As shown in Fig. 7, the maximum temperature is reached under the tool shoulder, where the tool has the most force and speed. As it turns out, as the cone angle increases, the temperature of the wires increases during the process. Increasing the temperature makes the material soft during the process and will significantly impact the quality of the wires produced.

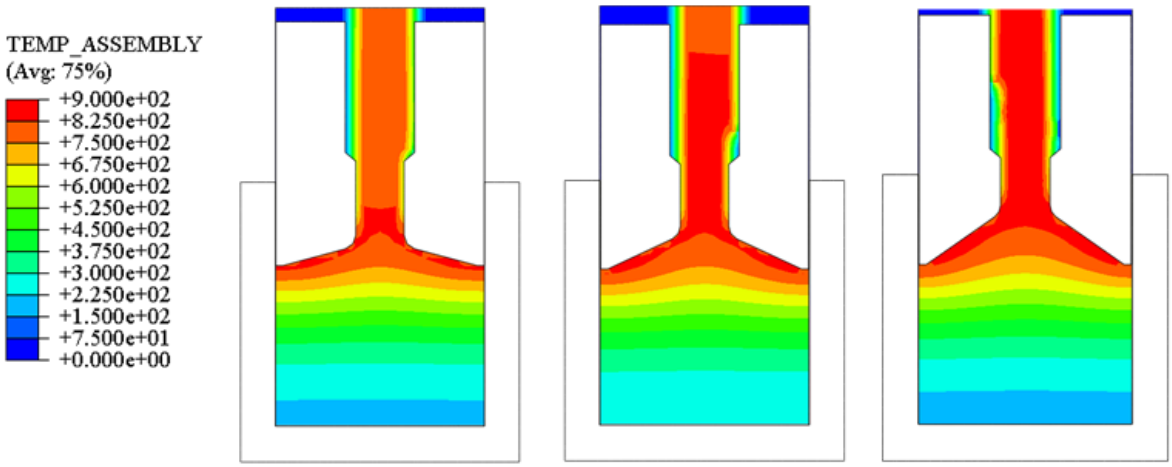

Fig.7
The material temperature during the process using a tool with a cone angle of a)15°, b)25°, c) 35°.

To more accurately investigate the effects of tool cone angle on the heat generated during the process and the resulting temperature, a numerical model was developed. As shown in Fig. 8, the tool consists of a conical and a horizontal surface.

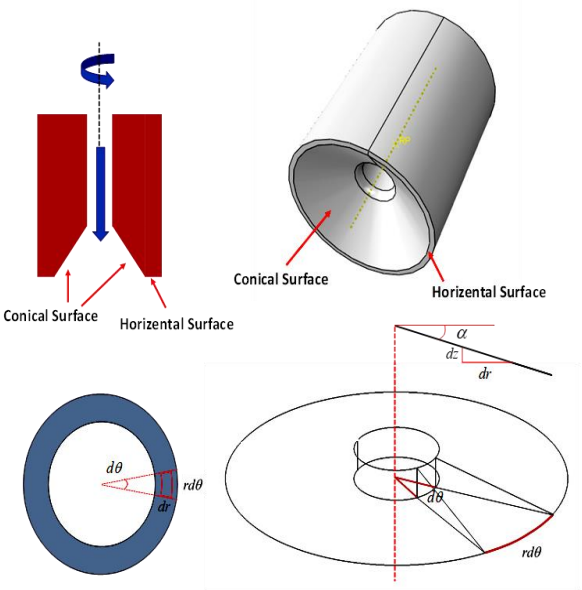

Fig.8
Schematic drawing of surface orientations and infinitesimal segment areas.

The heat generation expression varies depending on the surface orientation, but it is based on the basic heat generation equation [19]:

$$dQ = \omega dM = \omega r \tau_{contact} dA \tag{11}$$

where r is the distance from the investigated area to the center of rotation, ω is the angular velocity. The formula above approximates the heat created at the contact interface between the rotating tool and the material. The effects of tool linear velocity on temperature are not studied because the main factor in creating heat is the rotational motion of the tool. A specific tool surface in contact with the matrix is defined by its position and orientation in relation to the tool's rotation axis (Fig. 9).

If the tool rotation axis is in the direction of the Z-axis, then a flat surface of the tool would be horizontal or in the θr-plane. The following subscripts are used to indicate the orientation of the surface in the equations.

− =Horizontal (Perpendicular to the axis of rotation).

| =Vertical (Parallel to the axis of the tool rotation).

\ = Conical (the conical surface that tilted with respect to the rotation axis).

First, by selecting an infinitesimal segment on the tool surface, the heat created in the horizontal component of the tool is estimated. The area of this infinitesimal segment ($dA_{-} = rd\theta dr$) is subject to a uniform contact shear stress $\tau_{contact}$. This segment contributes with an infinitesimal force of $dF_{-} = \tau_{contact} dA_{-}$ and torque of $dM_{-} = rdF_{-}$. The heat generated from this segment is as follows:

$$dQ_{-} = \omega r dF_{-} = \omega r^2 \tau_{contact} d\theta dr \tag{12}$$

where $rd\theta$ and dr are the segment dimensions. By integrating this equation, the heat generated by the horizontal plane of the tool will be:

$$dQ_{-} = \int_0^{2\pi} \int_{R_{Slope}}^{R_{Tool}} \omega r^2 \tau_{contact} d\theta dr = \frac{2}{3} \pi \tau_{contact} \omega (R_{Tool}^3 - R_{Slop}^3) \tag{13}$$

After calculating the heat generated in the horizontal plane, the heat generated in the conical surface of the tool will be calculated. In fact, because the tilted segment area is projected onto the major planes relative to the tool rotation axis, the force/torque contribution from the tilted segment is split into vertical and horizontal components. The tilted orientation is characterized by the cone angle α, which is the angle between the horizontal ($r\theta$) plane and the segment orientation in the rz-plane.

$$dF_{\backslash} = dF_{-} + dF_{|} \tag{14}$$

The projection of the tilted segment area is given by:

$$dz = \tan\alpha dr \tag{15}$$

$$dA_{|} = rd\theta dz = rd\theta \tan\alpha dr \tag{16}$$

$$dA_{-} = rd\theta dr \tag{17}$$

where α represents the cone angle. Inserting these equations into Eq.(14) gives:

$$dF_{\backslash} = \tau_{contact} dA_{-} + \tau_{contact} dA_{|} = \tau_{contact} rd\theta dr(1 + \tan\alpha) \tag{18}$$

This can be interpreted as the fraction of tan α enlarging the segment area when compared to a horizontal segment. The modification of the heat generated at the tilted segment is:

$$dQ_{\backslash} = \omega r dF_{\backslash} = \omega r^2 \tau_{contact} d\theta dr(1 + \tan\alpha) \tag{19}$$

By integrating from this equation, the heat generated on the conical surface will be as follows:

$$dQ_{\backslash} = \int_0^{2\pi} \int_{R_{Hole}}^{R_{Tool}} \omega r^2 \tau_{contact} d\theta dr(1 + \tan\alpha) = \frac{2}{3} \pi \tau_{contact} \omega (R_{Tool}^3 - R_{Hole}^3)(1 + \tan\alpha) \tag{20}$$

The total heat generated is the sum of the heat generated in the horizontal and conical surfaces:

$$Q_{total} = Q_1 + Q_2 = \frac{2}{3}\pi\tau_{contact}\omega(R_{Tool}^3 - R_{Slop}^3) + \frac{2}{3}\pi\tau_{contact}\omega(R_{Tool}^3 - R_{Hole}^3)(1+\tan\alpha) \quad (21)$$

As it is known, the cone angle affects the heat generated by the tool, so that with increasing the amount of the cone angle, the heat produced increases. This increase in heat generated increases the temperature of the samples during the process, which justifies the simulation results.

Fig. 9 shows the force applied to the tool during the process. As can be seen, the force first increases rapidly to reach its maximum value and then is gradually reduced. Initially, the force increases due to the penetration of the tool into the material. After that, due to the heat generated in the material, the material softens and reduces the force on the tool. This reduction in force continues due to the increase in material temperature during the process [20]. Also, as can be seen, increasing the tool cone angle reduces the force on the tool. This reduction in force occurs for two reasons. On the one hand, by increasing the cone angle, the material enters more efficiently, and less surface is involved with the material at the beginning of the process. On the other hand, by increasing the cone angle of the tool, as seen, it increases the heat produced in the material, and thus the material becomes more soften [21]. This reduction in force has a significant impact on the life of the tool as well as the life of the milling machine and thus reduces costs.

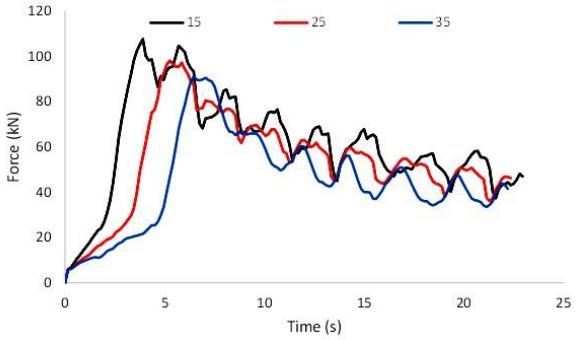

Fig.9
Force on the tool with different cone angles.

Fig. 10 illustrates the cross-section macrograph of the produced wire by FSBE. As it turns out, only tools with a cone angle of 35° were able to produce flawless wires. In the produced wire with a cone angle of 15°, many discontinuities can be seen on the outer surface of the wire. Also, in the wire produced with a cone angle of 25°, a hole is seen in the center of the wire, and the material does not appropriately fill this area. These defects reveal that inadequate heat generation leads to the poor formability of materials under process and then results in the generation of discontinuity in the sample core. As shown in the previous sections, the heat generated increases with increasing cone angle, which results in better flow of the material and thus eliminates defects such as cavities and discontinuities.

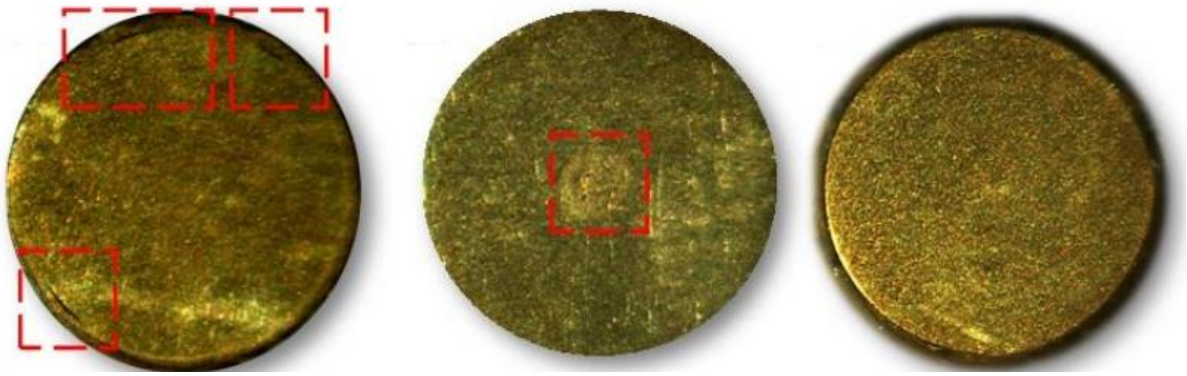

(a) (b) (c)

Fig.10
The cross-section macrograph of the produced by the tool with a cone angle of a)15°, b)25°, c) 35°.

After examining different tools, a tool with a cone angle of 35° was selected as a suitable tool for the production of brass wires. This tool produced flawless wires due to the production of more heat as well as the production of better material flow. Also, the force on the tool and consequently on the device, which is one of the limiting parameters in the process, is reduced when using this tool.

4.3 Microstructural and mechanical properties

The peripheral and central microstructures of the cross-section of the FSBE-produced wires are shown in Figs. 11(a) and 11(b). The periphery microstructure is more refined than the center microstructure, as indicated. This differential, which affects microhardness, is linked to the amount of strain and temperature encountered. [21].

In terms of strain, the materials at the wire periphery experience a higher amount of strain due to the higher linear velocity of the tool at the periphery rather than the tool center (Fig. 12(a)). It is well-known that increasing the strain increases the nucleation sites over the recrystallization and thus reduces the grain size in the produced microstructure.

Regarding the experienced temperature over the processing time, it could be declared that the surface of the FSBE tool acts as a heat well and cools the outer surface of the wires that are in contact with the tool, and as a result, the temperature at the surface of the wires is lower than the center of the wire (Fig. 12(b)). As a result, the lower experienced temperature at the wire periphery reduces the grain growth during the process. Higher strain and lower temperature of the outer surface of the wires is the main reason for the smaller grain size in this area.

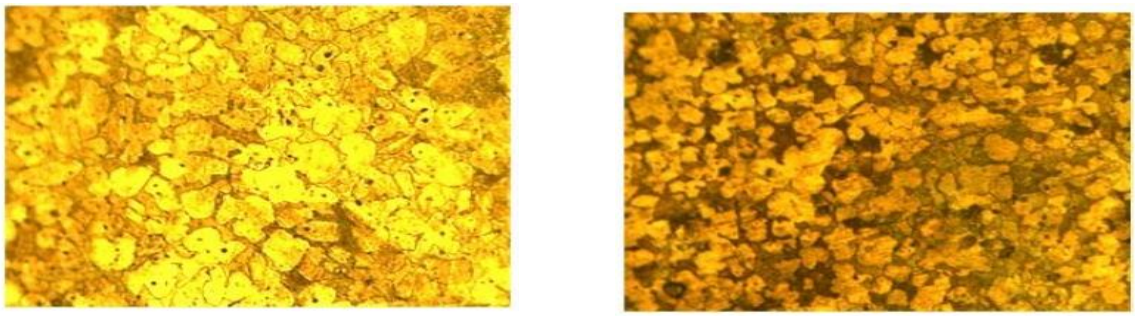

(a) (b)

Fig.11
Cross-section macro image of the produced brass wire by FSBE. (a) central and (b) peripheral microstructures of the sample.

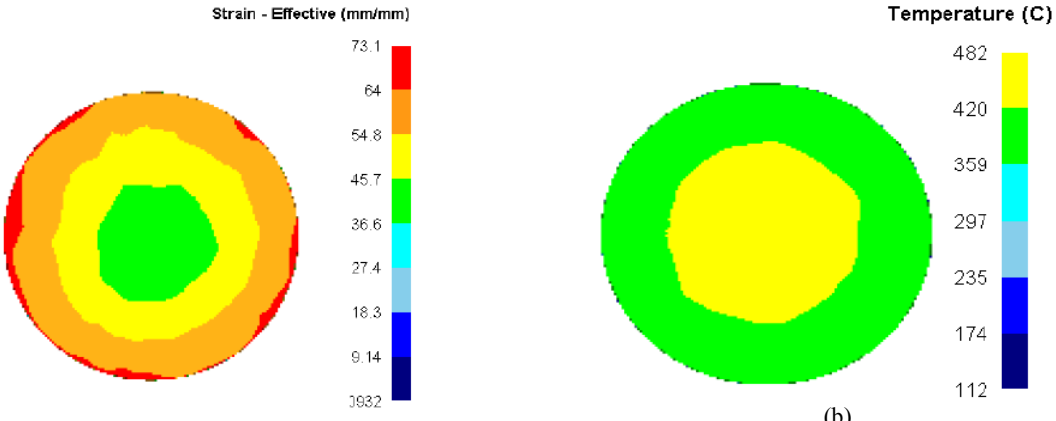

(a) (b)

Fig.12
a) Strain distribution and b) Temperature distribution on the cross-section of the wires.

According to the microstructural results, it is expected that the microhardness value at the sample periphery is higher than that of the sample center. The central microhardness for the sample is 119 *HV*, respectively, while its peripheral microhardness is 123 *HV*. The main reason for higher hardness at the sample peripheral is the grain size (Fig. 10). The engineering stress-strain pressure test curve for the sample is shown in Fig. 13.

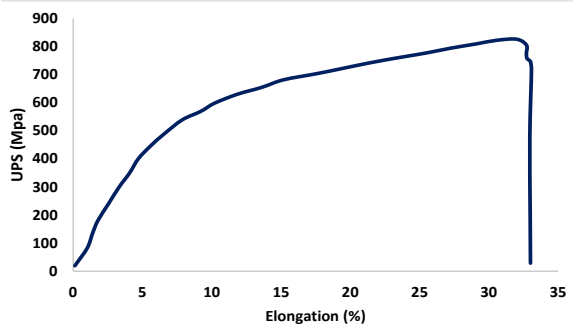

Fig.13
The engineering stress-strain pressure test curves for samples.

5 CONCLUSIONS

This research investigates the effect of tool cone angles on the wires produced during the FSBE process. For this purpose, first, the FSBE process was modeled using the CEL method, and the numerical results were validated with experimental results. Then, using macro images, defects in the wires were examined. In summary, the following results were obtained in this study:

- With increasing tool cone angle, the temperature of the material increased during the process due to the increase in the effective surface in heat production.
- The highest temperature and strain occur near the tool/workpiece interface but further from the tool axis.
- Increasing the tool cone angle reduces the force on the milling machine and machine and thus increases their life.
- For the manufacturing of brass wires, a tool with a cone angle of 35 degrees was chosen. Because of the increased heat generation and improved material flow, this instrument generated perfect wires.

The microstructure of a generated FSBE sample (wire) is more refined in the periphery than in the centre of the cross-section. This microstructural deviation is mainly affected by the strain and the temperature.

REFERENCES

[1] Heidarzadeh A., 2020, Application of nanoindentation to evaluate the hardness and yield strength of brass joints produced by FSW: microstructural and strengthening mechanisms, *Archives of Civil and Mechanical Engineering* **20**(2): 41.

[2] Heidarzadeh A., 2019, Tensile behavior, microstructure, and substructure of the friction stir welded 70/30 brass joints: RSM, EBSD, and TEM study, *Archives of Civil and Mechanical Engineering* **19**(1): 137-146.

[3] Xu N., 2020, Recrystallization of Cu-30Zn brass during friction stir welding, *Journal of Materials Research and Technology* **9**(3): 3746-3758.

[4] Saravanakumar S., 2020, Experimental analysis of dissimilar metal of copper and brass plates fabricated friction stir welding, *Materials Today: Proceedings* **33**: 3131-3134.

[5] Evans W.T., 2015, Friction stir extrusion: a new process for joining dissimilar materials, *Manufacturing Letters* **5**: 25-28.

[6] Buffa G., 2016, AZ31 magnesium alloy recycling through friction stir extrusion process, *International Journal of Material Forming* **9**(5): 613-618.

[7] Akbari M., Asadi P., 2020, Dissimilar friction stir lap welding of aluminum to brass: Modeling of material mixing using coupled Eulerian–Lagrangian method with experimental verifications, *Proceedings of the Institution of Mechanical Engineers, Part L: Journal of Materials: Design and Applications* **234**(8): 1117-1128.

[8] Akbari M., Asadi P., Behnagh R.A., 2021, Modeling of material flow in dissimilar friction stir lap welding of aluminum and brass using coupled Eulerian and Lagrangian method, *The International Journal of Advanced Manufacturing Technology* **113**(3): 721-734.

[9] Akbari M., 2017, Hybrid multi-objective optimization of microstructural and mechanical properties of B4C/A356 composites fabricated by FSP using TOPSIS and modified NSGA-II, *Transactions of Nonferrous Metals Society of China* **27**(11): 2317-2333.

[10] Tahmasbi K., Mahmoodi M., 2018, Evaluation of microstructure and mechanical properties of aluminum AA7022 produced by friction stir extrusion, *Journal of Manufacturing Processes* **32**: 151-159.

[11] Li J., 2021, Friction stir extrusion for fabricating Mg-RE alloys with high strength and ductility, *Materials Letters* **289**: 129414.

[12] Baffari D., 2017, Process mechanics in Friction Stir Extrusion of magnesium alloys chips through experiments and numerical simulation*, Journal of Manufacturing Processes* **29**: 41-49.
[13] Asadi P., Akbari M., 2021, Numerical modeling and experimental investigation of brass wire forming by friction stir back extrusion*, The International Journal of Advanced Manufacturing Technology* **116**: 3231-3245.
[14] Akbari M., Asadi P., 2021, Optimization of microstructural and mechanical properties of brass wire produced by friction stir extrusion using Taguchi method*, Proceedings of the Institution of Mechanical Engineers, Part L: Journal of Materials: Design and Applications* **235**(12): 2709-2719.
[15] Meyghani B., 2017, A comparison of different finite element methods in the thermal analysis of friction stir welding (FSW)*, Metals* **7**: 450.
[16] Chakrabarty R., Song J., 2020, A modified Johnson-Cook material model with strain gradient plasticity consideration for numerical simulation of cold spray process*, Surface and Coatings Technology* **397**: 125981.
[17] Balu Mahandiran M., 2021, Investigation of solid state welding of copper nickel alloy (Cu-Ni 90/10) using FSW process*, IOP Conference Series: Materials Science and Engineering* **1145**(1): 012112.
[18] Wang X., 2020, On the solid-state-bonding mechanism in friction stir welding*, Extreme Mechanics Letters* **37**: 100727.
[19] Schmidt H., Hattel J.H., Wert J., 2003, An analytical model for the heat generation in friction stir welding*, Modelling and Simulation in Materials Science and Engineering* **12**: 143.
[20] Akbari M., 2016, The effect of in-process cooling conditions on temperature, force, wear resistance, microstructural, and mechanical properties of friction stir processed A356*, Proceedings of the Institution of Mechanical Engineers, Part L: Journal of Materials Design and Applications* **232**(5): 429-437.
[21] Akbari M., 2015, Investigation of the effect of friction stir processing parameters on temperature and forces of Al–Si aluminum alloys*, Proceedings of the Institution of Mechanical Engineers, Part L: Journal of Materials: Design and Applications* **232**(3): 213-229.